Design of a Toroidal Fast-Field Cycling Nuclear Magnetic Resonance relaxometer's electromagnet

João Tiago Padrão Ribeiro da Cunha
Departamento de Física, CeFEMA, Instituto Superior Técnico, Lisboa, Portugal
(Dated: October 2020)

In this article, the design and development of a novel Fast-Field Cycling (FFC) Nuclear Magnetic Resonance (NMR) relaxometer's electromagnet is described. This magnet is tailored to increase the relaxometers's usability, by increasing its portability capacities. It presents a compact toroidal-shaped iron core, allowing to operate in a field range of 0 to 0.21 T, with high field homogeneity (less than 800 ppm in a volume of ≈ 0.57 cm^3), low power consumption and reduced losses (about 40 W). The simulation software COMSOL Multiphysics® is used to characterize the induced magnetic field, the heating and the cooling effects.
Keywords: Fast-Field Cycling, Nuclear Magnetic Resonance, NMR electromagnet, Portable NMR.

I. INTRODUCTION

Nuclear Magnetic Resonance (NMR) relaxometry is a powerful experimental technique, which has a diverse array of scientific research and industrial applications. The aim of this technique is to obtain detailed information about the molecular structure and dynamics of a given sample, from the interaction between the nuclear spins and their molecular environment [1].

In order to comply with the specific requirements of the multiple applications of NMR, different spectroscopy techniques have been conceived and employed over the years. Nonetheless, all of these techniques are based on the same principle: a nuclear spin system exposed to a strong, static, magnetic field ($\vec{B}_0$), and perturbed by radio frequency (RF) pulses in resonance with the Larmor frequency ($\omega_0 = \gamma B_0$) of that system, will respond by absorbing and re-emitting electromagnetic radiation (i.e. producing an electromagnetic signal) with that characteristic frequency.

The particular NMR technique explored in this work is known as Fast-Field Cycling (FFC). It originated from the fact that using the more conventional relaxometry techniques (such as inversion-recovery) it is very impractical, or even impossible, to perform studies at lower magnetic fields (i.e. at lower frequencies, according to the Larmor equation). This is due, mainly, to the decrease of the signal-to-noise ratio at low fields. Yet, the FFC technique allows to overcome this weakening of the NMR induction signal at lower fields by placing the sample under the influence of a cyclic magnetic field. Doing so, it becomes possible to execute measurements at a low intensity field, but with the signal acquisition only being performed at a higher intensity field (and thus with a good signal-to-noise ratio).

To implement this technique certain requirements need to be fulfilled, demanding the use of specific relaxometers. Among other factors, it is necessary to guarantee a fast, but stable, modulation of the induced magnetic field $\vec{B}_0$, which also has to be as homogeneous as possible. For this reason, most FFC relaxometers currently employ air-cored solenoid magnets, which allow to produce high homogeneity fields, with relatively low inductance and resistance. However, due to the relatively low magnetic permeability of air, the generation of a sufficiently strong magnetic field is very energy consuming. As a consequence, complex cooling systems are required to dissipate, in some cases, several kW [2].

This circumstance can be rather problematic since FFC experiments are very sensitive to the thermal stability of the magnets, which can affect the intensity of the magnetic fields and the switching times between field levels. In situations where the cooling system is not able to stabilize the temperature of the magnet, it becomes necessary to have certain periods during the relaxometry field cycles where the magnet power is reduced to very low values. This introduces a considerable constraint in cases where the magnet induces molecular alignment in the sample, since, during these low power periods, the molecular alignment will obviously be disturbed [3]. One of these particular cases is that of liquid crystals, which is one of the main areas of focus of the research group at IST.

A possible solution to reduce power and cooling demands, and decrease operating costs, is to use ferromagnetic materials to form the magnet's core. Such materials present magnetic permeabilities significantly higher than that of air, establishing therefore a medium where the magnetic flux can be magnified. As a result, electrical current (and, thus, cooling) demands are considerably reduced. This is precisely the approach followed in this work, with the design of an iron-cored magnet.

In recent years, a growing interest in NMR relaxometry techniques, and their vast applications, has been observed worldwide. This is particularly true for techniques such as Magnetic Resonance Imaging (MRI) or high resolution NMR, which have become highly coveted tools in the non-academic world, thus motivating the development of new, more advanced, equipments. However, the same cannot be said about FFC NMR relaxometry, where the existing FFC relaxometers do not yet possess all the desired qualities, being too expensive, bulky and having high power demands. There is still, therefore, a

lot of room for progress in the area, particularly as NMR relaxometry progresses towards becoming more portable, with more practical applications outside of a laboratory environment. As this new trend of *in situ* studies starts to emerge and establish itself in the world of NMR, it becomes pressing to develop the first portable relaxometers specifically designed to employ the FFC technique. To that end, in this work, an innovative FFC NMR magnet is projected and described, being our ambition that this magnet will be the genesis of portable FFC relaxometry.

II. THEORETICAL BACKGROUND

A. Nuclear Magnetic Resonance

Spectroscopy is, simply put, the study of the interaction between matter and electromagnetic radiation. It allows to examine and understand the properties of a sample by analysing the absorption/emission of radiation in terms of frequency. The physical phenomenon of Nuclear Magnetic Resonance is a type of spectroscopy. It occurs when nuclei of certain atoms immersed in a strong static magnetic field are exposed to a second, oscillating, magnetic field, and react by producing an electromagnetic signal with a characteristic frequency [4]. This signal is measured and processed in different ways, yielding a NMR spectrum through which the discrimination and identification of the nuclear constituents of a sample is possible.

NMR studies are based on the properties of the nucleus of atoms, particularly on spin and magnetic quantum numbers, and their behaviour when subjected to magnetic fields. This technique measures the interaction energy between magnetic nuclear moments and magnetic fields. In classical terms, in the presence of a magnetic field, a magnetic moment will naturally precess. The frequency of this motion depends on the environment that surrounds the nucleus, i.e., it will depend on the interactions of the magnetic moments with the surrounding magnetic fields. These interactions are what allows NMR to analyse in a particularly detailed way the structure and molecular dynamics of a sample.

However, not all atoms can be used to conduct NMR studies. In fact, only those with non-zero nuclear spin, which occurs for all isotopes with an odd number of protons and/or neutrons, are susceptible to magnetic stimulus and therefore suitable for NMR [5].

B. Nuclear Spin

The nucleus of an atom consists of two particles, protons and neutrons. These particles have an intrinsic property known as spin, a form of angular momentum analogous to the classical angular momentum of a rotating object. The overall nuclear spin angular momentum (which can be thought of as a vector $\vec{I}$) is determined by the spin quantum number I. Furthermore, all nuclei with non-zero spin $\vec{I}$ have a dipolar magnetic moment $\vec{\mu}$, collinear with it, given by [6]:

$$\vec{\mu} = \gamma \vec{I} \quad (\mathrm{Am}^2), \tag{1}$$

where γ is the gyromagnetic ratio, and $\hbar$ is the reduced Planck constant. The magnetic energy associated to each nucleus when subjected to a magnetic field $\vec{B}_0 = B_0\vec{e_z}$, depends on the magnitude of its spin and on the field intensity, according to [4]:

$$E = -\vec{\mu} \cdot \vec{B}_0 = -\gamma \hbar I_z B_0 = -\gamma m \hbar B_0 \quad (J), \tag{2}$$

with $I_z = m$ being the quantum number describing the different orientations of the spins with respect to the external field. Since for each spin-I nuclei there are $2I + 1$ degenerate states, with an associated magnetic quantum number, $m = -I, -I+1, ..., I-1, I$, the energy is quantized (e.g., a nucleus with spin $I = 1/2$, has two possible energy levels, while if it has spin I=3/2, it will then have four possible energy levels [7]).

Because the only allowed transitions are the ones that respect $\Delta m = \pm 1$, the amount of energy involved in the process is always the same: $\Delta E = \gamma \hbar B_0$. This energy difference between adjacent levels defines the Larmor frequency, ω_L:

$$\omega_L = \gamma B_0 \quad (rads^{-1}), \tag{3}$$

whose value depends on the magnetic field intensity applied on the nucleus.

C. Magnetization

In the absence of a magnetic field, all the elementary spin moments in a sample are randomly oriented in space, resulting in zero magnetization. However, when an external magnetic field $\vec{B}_0 = B_0\vec{e_z}$ is applied to the sample, the spins change their orientations, aligning with the direction of that field. The spins not only respond to the imposed magnetic field, but also interact with each other, ending with different equilibrium orientations. This leads to the rise of a net magnetization, $\vec{M}$, which results from the contributions of all the nuclear magnetic moments, $\vec{\mu_i}$ [6]:

$$\vec{M} = \frac{\sum_i \vec{\mu_i}}{V} \quad (Am^{-1}), \tag{4}$$

where V is the volume of the sample.

D. Relaxation

Classically, a nuclear spin magnetic moment, $\vec{\mu}$, will naturally precess when exposed to an external magnetic

field, such as $\vec{B}_0 = B_0\vec{e}_z$, due to the forces (the torque) created by such field. This precession movement is described by a torque, which also corresponds to the rate of change of the angular momentum [8]:

$$\vec{\tau} = \vec{\mu} \times \vec{B}_0 = \frac{d\vec{I}}{dt} \quad \text{(Nm)}. \tag{5}$$

Since, from equation (1), $\vec{I} = \vec{\mu}/\gamma$, the previous equation reads:

$$\frac{d\vec{\mu}}{dt} = \gamma(\vec{\mu} \times \vec{B}_0) \quad (\text{Am}^2\text{s}^{-1}). \tag{6}$$

Therefore, given that $\vec{M}$ is the vector sum of the magnetic moments (as seen in equation (4)), by summing equation (6) vectorially over all $\vec{\mu}$ we obtain the following relation for the magnetization:

$$\frac{d\vec{M}}{dt} = \gamma(\vec{M} \times \vec{B}_0) \quad (\text{Am}^{-1}\text{s}^{-1}). \tag{7}$$

which shows that the net magnetization performs a precession around the direction of B_0 at the Larmor frequency [9].

If, however, a second, time-oscillating, magnetic field $\vec{B}_1$, perpendicular to $\vec{B}_0$, is applied, the system is disturbed, resulting in a loss of alignment between $\vec{B}_0$ and the net magnetization. Considering that $\vec{B}_1$, usually applied in the form of radio frequency (RF) pulses, is tuned to the Larmor frequency, state transitions are induced in the sample. In this case, when the RF pulse is applied, the net magnetization tips from the longitudinal axis to the transverse plane, rotating at the Larmor frequency. The flip-angle, i.e., the angle between the tipped magnetization and the z-axis, is [8]:

$$\alpha = \gamma B_1 t_{pulse} \quad (rad), \tag{8}$$

with t_{pulse} being the length of the pulse. The intensity and length of the RF pulse determine the amount of energy supplied to the spin system, therefore determining the flip-angle. Typically, $\pi/2$ and π pulse sequences are used to flip the magnetization by 90 and 180 degrees, respectively.

Assuming then that at equilibrium $\vec{B}_0 = B_0\vec{e}_z$ and $\vec{M} = M\vec{e}_z$, after a perturbation such as a $\pi/2$ RF pulse is applied, the magnetization flips to the xy-plane, and immediately starts to recover to its initial value along the applied external magnetic field $\vec{B}_0$, in a process known as relaxation. During this process, part of the energy previously absorbed by the nuclei is emitted in the form of a weak electromagnetic field, that can be detected by an antenna, and is known as "Free Induction Decay" (FID). This process is represented in Fig. 1.

The complete set Bloch equations, describing the behavior of the magnetization under the influence of the total magnetic field $\vec{B} = \vec{B}_0 + \vec{B}_1(t)$, and when subjected to relaxation processes, are presented in equation (9) [9].

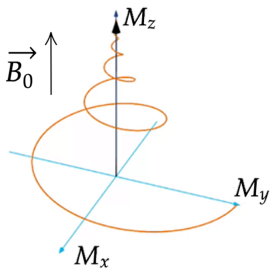

FIG. 1. Relaxation process. Realignment of the net magnetization with $\vec{B}_0$, after a $\pi/2$ pulse. Adapted from [10].

$$\begin{cases} \dfrac{dM_x}{dt} = [\vec{M} \times \gamma\vec{B}]_x - \dfrac{M_x}{T_2}, \\ \dfrac{dM_y}{dt} = [\vec{M} \times \gamma\vec{B}]_y - \dfrac{M_y}{T_2}, \\ \dfrac{dM_z}{dt} = [\vec{M} \times \gamma\vec{B}]_z - \dfrac{M_z - M_0}{T_1}. \end{cases} \tag{9}$$

The time constants T_1 and T_2 are related to the realignment of nuclei magnetization with the static external field, and are known as relaxation times [11].

T_1, the spin-lattice (or longitudinal) relaxation time, quantifies the rate of transfer of energy from the nuclear spin system to the environment. It is the time constant for the physical processes responsible for bringing the longitudinal component of the magnetization vector $\vec{M}$ back to its equilibrium position, parallel to the external field $\vec{B}_0$.

T_2, the spin-spin (or transversal) relaxation time, accounts for the transfer of energy between neighbouring nuclei, and is connected to the loss of coherence of the magnetization in the transverse direction. Fluctuations of the local magnetic field (due to inhomogeneity) lead to random variations in the instantaneous NMR precession frequency of different spins. As a result, the initial phase coherence of the nuclear spins is lost, until eventually the phases are disordered and there is no net magnetization in the xy-plane.

Thus, after a $\pi/2$ pulse, the magnetization in the xy-plane, which had reached its maximum value immediately after the pulse, will decrease on the xy-axis, returning to zero. At the same time, the z-component of the magnetization, which was null after the pulse, starts to recover until it is back to its initial state (see Fig. 1).

III. FAST-FIELD CYCLING

In a typical FFC NMR experiment the sample is initially placed in a magnetic field $B_{0,p}$, where it is polarized for a time Δt_p. This field, which typically defines the z-axis, must be strong enough to align the nuclear spin magnetization of the sample with that axis,

i.e., $\vec{M} = M\vec{e_z}$. Following this polarization, the magnetic field is switched down to a lower field value $B_{0,e}$. The goal is to polarize the sample as much as possible, so that the intensity of the magnetization signal can be boosted, and then to let the magnetization evolve (also along the z-axis) to a new equilibrium, after quickly ($t_{switching} \ll T_1(B_{0,e})$) switching the field from $B_{0,p}$ to $B_{0,e}$.

After a certain evolution time Δt_e, a new higher intensity field, known as the detection field $B_{0,d}$, is applied, immediately followed by a $\pi/2$ RF pulse that rotates the magnetization to the xy-plane (where the FID signal can be detected) ([11], [12], [13]).

To properly observe the behaviour of the nuclear spin system, several cycles need to occur with varying experimental parameters. Thus, after a cycle, a recycle delay follows, allowing for the reset of the polarization and thermal equilibrium, so that the next cycle can begin.

This technique allows the magnetization to reach its asymptotic value via relaxation at a low intensity field, which can be set to any desired value, while the signal detection is still performed at a high intensity field [5], which is crucial in order to have a good signal-to-noise ratio. In Fig. 2, a representation of this cycle can be seen.

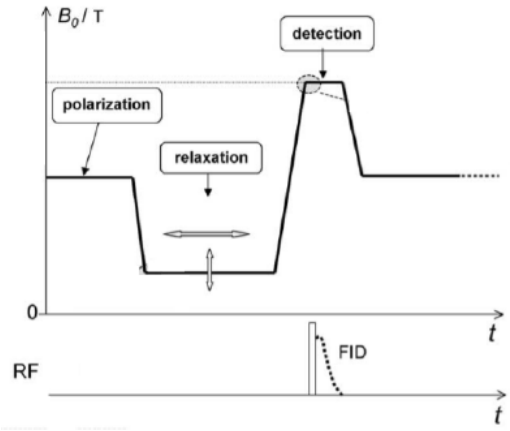

FIG. 2. Typical FFC relaxometry cycle. Adapted from [5]

In order to determine the value of T_1, we assume that the evolution of the magnetization can be correctly described by the Bloch equations (9), and that the transitions between magnetic fields are fast enough so that no relaxation occurs in that period. However, these transitions cannot be arbitrarily fast, since it is also necessary to guarantee the adiabaticity of the evolution of the magnetization, i.e., that no perpendicular components to $\vec{B_0}$ appear during magnetic field transitions [14].

Ideally, one would want to measure T_1 for the magnetic field $B_{0,e}$, since this lower field allows to detect and analyze even the slower molecular motions. However, this also means having a poor signal-to-noise ratio, as we have already seen. This way, the detection of the FID signal only happens after the transition to the higher intensity field $B_{0,d}$. Nonetheless, it is possible to demonstrate that, if some experimental conditions are assured, the value of the magnetization (immediately before the RF pulse is emitted, in the detection phase) is proportional to the value of the magnetization at the end of the evolution phase. Hence, we will retain the information from the nuclear magnetization in the sample at lower fields, but the detection is performed at a high field, therefore, with a better S/N. By changing the moment at which the RF pulse is emitted, the FID signal, proportional to the magnetization, will be different, allowing to determine $T_1(B_{0,e})$, as intended ([11], [12]).

IV. THE MAGNET SYSTEM

The main component of a FFC relaxometer is the magnet system. As the ultimate purpose of this project was the development of a portable FFC relaxometer, a magnet with very particular characteristics was created. Its defining one is the capacity to freely rotate over all three axis. This allows to have easier access to the samples by being able to adapt the relaxometer to them, instead of the opposite, thus reducing the level of interference with their natural state. To that end, it was decided that the most suitable geometry for the magnet's core was that of a torus, with a gap on one of its sides for sample insertion. The coils are wound over this structure, being distributed symmetrically around it (see Fig. 3).

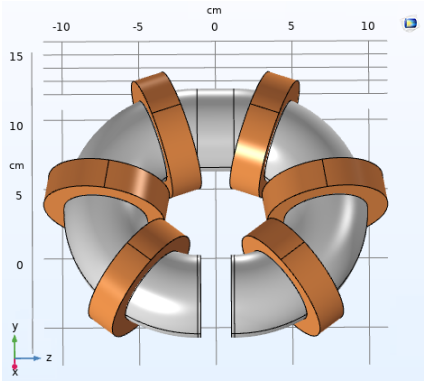

FIG. 3. Envisioned magnet system specially designed to increase the relaxometer's portability. The coils are represented in brown, and the core in grey.

As mentioned before, this core is made of iron, which presents a relatively high permeability (of the order of 1000, compared with just 1 for air). This means that the iron core provides a path of much less resistance than air for the magnetic field lines to pass through, supporting the development and magnification of the magnetic flux. The core is also a fundamental structural component of the magnet, as it serves as the physical support for the coils. In terms of its composition, to reduce core losses, instead of using a solid iron core two different approaches were studied: use iron fillings to form the core, or create a laminated core using thin iron sheets.

To define the magnet's parametric configuration, a series of simulations were performed using COMSOL Multiphysics®. The objective of these simulations was to evaluate the impact that every controllable parameter had on the magnet's characteristics, thus allowing to establish an optimal equilibrium between them.

The main observations/results obtained for each of the analyzed parameters are summarized in the following list:

- **Iron core dimensions**: The dimensions of the iron core greatly influence the characteristics of the induced magnetic field in the sample site, namely its intensity and homogeneity. Two parameters were evaluated: the radius of the toroidal iron core and its tube radius. On one hand, the greater both these dimensions were, the more intense and homogeneous was the magnetic field. On the other hand, greater dimensions meant larger size and weight of the magnet, which went against the objective of increasing its portability.

- **Number of coils**: It was rather straightforward to understand that, if everything else remained constant, the more coils were used, the stronger would be the induced magnetic field. However, with more coils other limitations arose, such as a decrease of available space and more severe cooling requirements. It was also concluded that, to reach the required field intensity of ≈ 0.21 T in the sample site, it would be preferable to use more coils with smaller dimensions (less turns per coil) than less coils with larger dimensions. Doing so, the homogeneity in the sample site increased, while the power demands and the inductance of the coils decreased.

- **Number of turns per coil**: The intensity of the induced magnetic field was directly related to the number of turns per coil. Nonetheless, as seen in the previous point, it was preferable to slightly decrease the number of turns per coil, while increasing the total number of coils. In fact, as the number of turns determines the height and width of the coils, more turns resulted in larger coils, which in turn caused the power demands (and Joule losses) to increase.

- **Coils position**: The position of the coils relative to the sample gap was found to affect the homogeneity and intensity of the field in the sample site. For homogeneity reasons, a certain minimum distance had to be kept between the first coil in each side of the core and the gap. Nonetheless, if the coils were placed too far from the gap, the field intensity and homogeneity would also decrease, as more leakage would occur throughout the core. Also, some distance had to be kept between consecutive coils, to increase the cooling efficiency of the magnet system.

- **Sample gap length**: It was concluded that the smaller the gap was, the higher was the intensity and homogeneity of the magnetic field in the sample site. On the other hand, considering the objective of increasing the magnet's usability capacities, the gap should be as large as possible, so as to allow for bigger, more varied samples to be studied. It was also necessary to take into account that the gap length limits the width of the coils, since they are inserted (and removed) through the gap.

As we were striving to increase the relaxometer's usability, our first priority was to keep the overall dimensions and weight of the magnet system as small as possible. Nonetheless, the gap had to be sufficiently large to give us enough flexibility in terms of sample diversity. Additionally, the homogeneity and intensity of the induced magnetic field still had to fulfill minimum quality parameters, to ensure a satisfactory level of performance of the magnet.

Taking all this into consideration, the optimal magnet configuration was eventually established, being presented in Table I.

Gap length [cm]	2
Torus radius [cm]	6
Number of coils	6
Turns per coil	146
Coil width/height [cm]	2/1.3

TABLE I. Optimal parametric configuration of the magnet system.

Note that this configuration was the same for the two studied types of core (fillings core and laminated core), with the only difference between them being the tube radius, which increased from 2.5 cm in the fillings core magnet to 2.9 cm in the laminated core magnet.

To reach the conclusion that these were indeed the optimal magnet configurations, for each of the various combinations of magnet parameters that were tested, magnet characteristics like the field homogeneity in the sample site, the coils inductance, the core weight/volume, and the core power losses were calculated. Additionally, multiple plots describing the induced magnetic field were analyzed. An example of one of those plots is presented in Fig. 4, where a detailed view of the magnetic field inside the iron core is shown, along with a surface plot of the magnetic field in the middle of the sample gap.

As expected for a toroidal core geometry, this plot shows that the field is more intense on the inside of the torus, particularly in the zones where the coils were placed. Near the sample gap the magnetic field reaches its lower intensity, which is also expected being that this is the point furthest away from any coils. The well-defined field map attests to the high homogeneity of the magnetic field in the sample site.

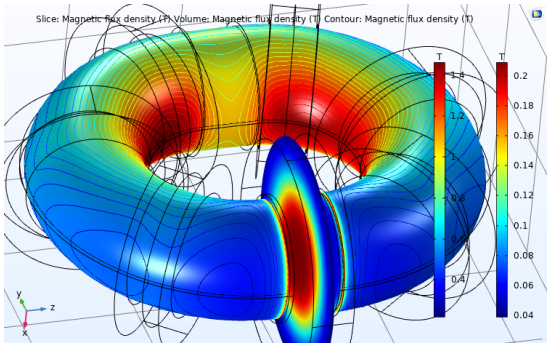

FIG. 4. Volume, contour and slice plots describing the magnetic field inside the core and in the sample gap of the fillings core magnet system.

V. FIELD HOMOGENEITY

The homogeneity of the induced magnetic field depends on the field variation and on the nominal value of the field, B_0, in a given volume, being expressed as:

$$H = \frac{\Delta B}{B_0} = \frac{B_{max} - B_{min}}{B_0}, \tag{10}$$

where B_{max} and B_{min} are, respectively, the maximum and minimum magnetic fields observed in that volume.

The necessity of having a field as homogeneous as possible arises from the fact that such a field can give us a much sharper and distinctive resonance line, since the energy is absorbed at a single frequency (the RF pulse precisely matches the sample Larmor frequency), instead of being absorbed over a band of frequencies (which happens when the field is not uniform over the sample). In turn, this makes it easier to discern the physical and chemical properties of a sample.

As a way to increase field homogeneity, the shape of the core poles was slightly modified. The idea was to carve an indentation in the poles (see Fig. 5) that would force the field lines to "curve" closer together, thus increasing field uniformity.

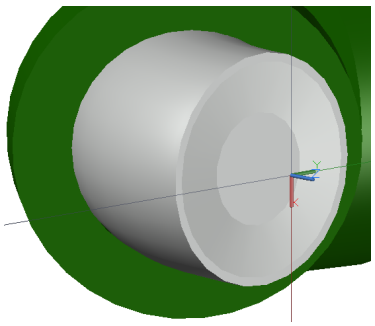

FIG. 5. Detail of the customized core pole.

To test the validity of this idea, the field homogeneity was studied for magnet systems with and without the customized poles, and the results compared. This homogeneity analysis was performed for two distinct volumes: volume $V_1 \approx 0.57$ cm^3, which corresponded to a cylinder of radius $r_1 = 0.6$ cm and height 0.5 cm; and volume $V_2 \approx 9.82$ cm^3, which corresponded to a cylinder of radius $r_1 = 2.5$ cm and height 0.5 cm.

To properly evaluate these homogeneous volumes, the induced magnetic field was characterized in three planes parallel to the core poles section: the middle plane of the gap ($z = 0$ cm), and two equidistant planes in $z = \pm 0.25$ cm. In each of the planes, two circular areas were examined, corresponding to the sections of the two cylindrical volumes (i.e., one circular area A_1 of radius $r_1 = 0.6$ cm for the smaller volume, and another circular area A_2 of radius $r_2 = 2.5$ cm for the larger volume).

An example of the plots used to characterize the induced field can be seen in Fig 6, where contour plots of the magnetic field in plane $z = 0$ cm of the fillings core magnet system (with and without customized poles) are presented.

Observing these plots it is clear to see that, for both types of poles, there is much higher homogeneity in the smaller area than in the larger one, as could be predicted. Note also that the contour plots suggest that the homogeneity is higher (at least for the smaller area) with the customized poles, given that for this type of poles no contour lines are contained inside the smaller area, which is not true for the smooth poles. Thus, the customized poles seem to be fulfilling their objective.

These same plots were performed for the other two planes (i.e., planes $z = \pm 0.25$ cm), of both the fillings core and the laminated core magnets, and the results were identical. It was also possible to observe that the field homogeneity, in each plane and for both types of pole, of the laminated core magnet system appeared to be higher than the one of the fillings core magnet system. Due to the larger dimensions of the laminated iron core in comparison with the iron fillings core (for the laminated core the tube radius is 2.9 cm, while for the fillings core is 2.5 cm), this result was expected.

The previous conclusions were confirmed by the magnetic field measurements that were performed in both areas (in the nine points represented in Fig. 6 **(a)**) of the three planes. Using this data, it was subsequently possible to calculate the homogeneity in both volumes (of each considered magnet). These homogeneity values are presented in Table II.

The results expressed in Table II are in accordance with what was predicted. It is possible to verify that, in each case, the field homogeneity in the smaller volume is significantly higher than in the larger volume. The idea that larger core dimensions have a positive impact in the homogeneity was corroborated by the fact that the laminated core (which has a larger tube radius) always presented higher homogeneity than the fillings core. Additionally, it was confirmed that the introduction of the customized poles served its purpose, given that, in all considered cases, the homogeneity with these poles was

			V_1 ($\approx 0.57\ cm^3$)		V_2 ($\approx 9.82\ cm^3$)	
		$B_{max} = B_0$ $[T]$	B_{min} $[T]$	$\frac{\Delta B}{B_0}$ [%]	B_{min} $[T]$	$\frac{\Delta B}{B_0}$ [%]
Fillings Core	**Smooth Poles**	0.20902	0.20831	0.340	0.16093	23.007
	Customized Poles	0.20890	0.20881	0.043	0.16949	18.865
Laminated Core	**Smooth Poles**	0.20852	0.20836	0.077	0.19002	8.872
	Customized Poles	0.20863	0.20856	0.034	0.19815	5.023

TABLE II. Analysis of the magnetic field homogeneity in the two cylindrical volumes of each considered magnet system.

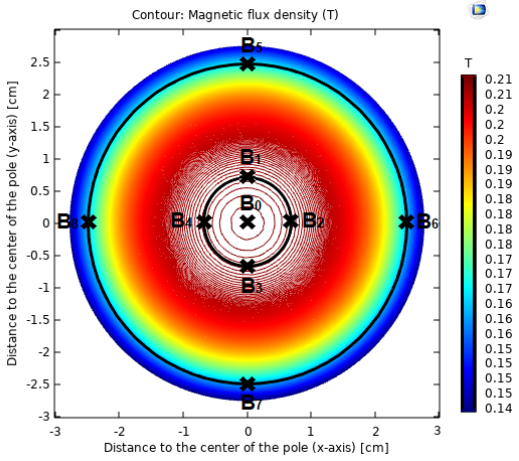

(a)

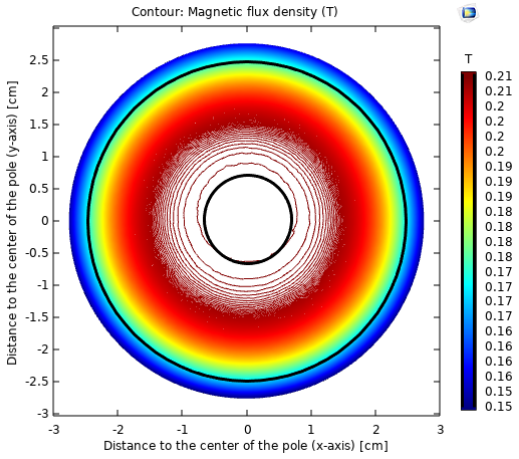

(b)

FIG. 6. **(a)/(b)** Contour plot in plane $z = 0$ cm, for, respectively, the smooth and the customized poles case (of the fillings core magnet). The black circles correspond to the two considered circular areas. Note also, in **(a)**, the nine points where the magnetic field was measured.

higher than with the normal, smooth poles. As such, from a results standpoint, this modification should be pursued when developing the magnet systems. However, implementing the customized poles in the laminated core would be extremely difficult from a technical standpoint, as it would require specialized work to carve the indentations directly on the metal sheets. Thus, it was decided that it would only be worth to introduce the customized poles for the fillings core magnet system, while keeping the smooth poles for the laminated core magnet system.

VI. FRINGING EFFECT

As the magnetic flux alternates between iron and air in the gap region, the flux lines start to become less and less parallel as one moves away from the center of the poles. At the edges of said region the fringing effect starts to be noticeable, leading to a decrease of field uniformity throughout the gap. This happens due to the fact that the permeability of air in the gap region is the same as the permeability of air everywhere else (outside of the core), with their reluctances also being similar. Thus, the flux is shared between the air gap and the neighbouring air volume around it (see Fig. 7). In other words, the flux lines will not be limited to an area A_c corresponding to the section area of the core poles, but rather they will be distributed in a larger fringing area A_f.

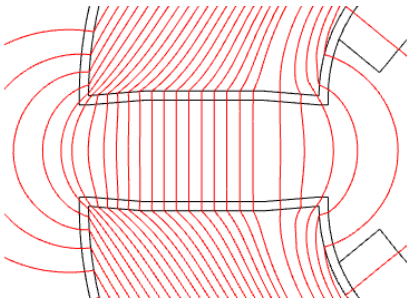

FIG. 7. Detail of the flux lines in the gap region and surrounding air volume, where the fringing effect is noticeable.

The fringing effect is quantified by a parameter known as the fringing factor, F_f. Different empirical formulas have been developed to calculate this factor, including one introduced by Roque [14] that follows:

$$F_f = 1 + \frac{A_f B_f}{A_c B_g}, \tag{11}$$

where B_g and B_f are, respectively, the average magnetic fields in areas A_c and A_f.

Performing simulations for varying gap lengths, it was possible to plot the evolution of the magnets' fringing factor as a function of the gap length using this formula. This is represented in Fig. 8, where *Cunha 1* corresponds to the evolution of the friging factor for the fillings core magnet system (with customized poles), while *Cunha 2* corresponds to that same evolution for the laminated core magnet system (with smooth poles). Furthermore, that evolution was compared with the ones obtained for the previous magnets developed by the IST research group (by Roque [14] and Videira [15]).

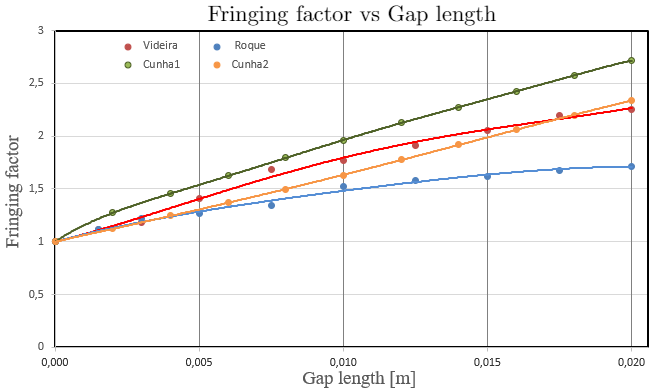

FIG. 8. Fringing factor as a function of the gap length for the fillings core magnet system with customized poles (*Cunha 1*) and for the laminated core magnet system with smooth poles (*Cunha 2*). Comparison with the same plot for the two previously developed magnets (*Roque* and *Videira*).

It is possible to see that our magnets (particularly the fillings core one) present higher fringing factor at the treated gap length of 2 cm than the other two magnets. This may be explained by the different geometry of the magnet systems. In fact, the magnet systems developed by both Roque and Videira used H-shaped magnetic cores. Our magnet systems, on the other hand, used a toroidal-shaped iron core. As such, due to its shape, not only had the flux lines to travel a longer (and curved) path inside the core, but the coils were also placed further away from each other (and from the gap). This caused the leakage flux to be higher than in the previously developed magnets: in our case, it was about 50% of the total flux, while for Videira's it was closer to 40%, and Roque's to 10% (due to the use of superconductors). As a consequence of the increased leakage, the fringing region, and in turn the fringing factor, also increased.

VII. HEATING AND COOLING OF THE MAGNET SYSTEM

Creation of the magnetic field inevitably leads to heating effects in the magnet system, due, mainly, to Joule losses in the coils. It is fundamental to properly characterize these effects, in order to minimize any type of negative impact that they may have in the system, such as structural damage (melting, ...) of its components, by setting-up an adequate cooling system.

The study of the heating effects was performed only for the magnet system with higher Joule losses, which was the fillings core magnet system. By considering this case it was possible to overestimate the cooling requirements, guaranteeing the design of a reliable cooling system.

For this magnet system, the simulated Joule dissipation losses were close to 60 W, for an applied current of 5 A. Technically speaking, this maximum current would only be applied to produce the maximum intensity fields of the fast field cycle (i.e., the polarization and detection fields). However, for simulation purposes, this current was considered constant, which was also a source of overestimation of the cooling requirements. The result of the stationary study performed can be observed in Fig. 9 **(a)**, showing the equilibrium temperature of the magnet system without cooling.

It can be observed that, in the absence of a cooling system, the magnet reaches an average equilibrium temperature of around 390 °C. This high equilibrium temperature makes it clear that it would not be viable to operate the magnet system without a proper cooling system. Otherwise, it would not be possible to manage the dissipated heat, and damage to the components of the magnet would certainly occur.

Taking this into consideration, a cooling system was simulated, which basically consisted of an air flow that removed the excess heat from the magnet system, allowing it to work within a safe temperature range. The defined cooling problem can be summarized as follows: the magnet system was composed of six coils, which dissipated a total of about 60 W; the initial temperature of the system was 20 °C, but the heating effects caused the temperature to rise to around 390 °C; to remove the excess heat, a laminar air flow was forced into the system by a fan, at a flow rate of 0.03 m^3/s and a temperature of 20 °C; this flow passed through the entire geometry, cooling the system before exiting it via two grilles.

Observing Fig. 9 **(b)**, which shows the equilibrium temperature of the system after the cooling effects, allows to conclude that the air flow method was successful in removing the excess heat produced by the coils, as an average equilibrium temperature of around 24 °C is reached. This guarantees that, for a cooling flow rate of 0.03 m^3/s, the magnet system is capable of operating for prolonged periods of time without damage to its components. Note that different flow rates could have been considered, as there are multiple available fans in the market that can be employed in this system. An increased flow rate would allow to remove more excess heat and, consequently, reduce even further the equilibrium temperature of the system. This would, however, come with an increased energy cost, so that this balance needs to be better evaluated when developing the relaxometer.

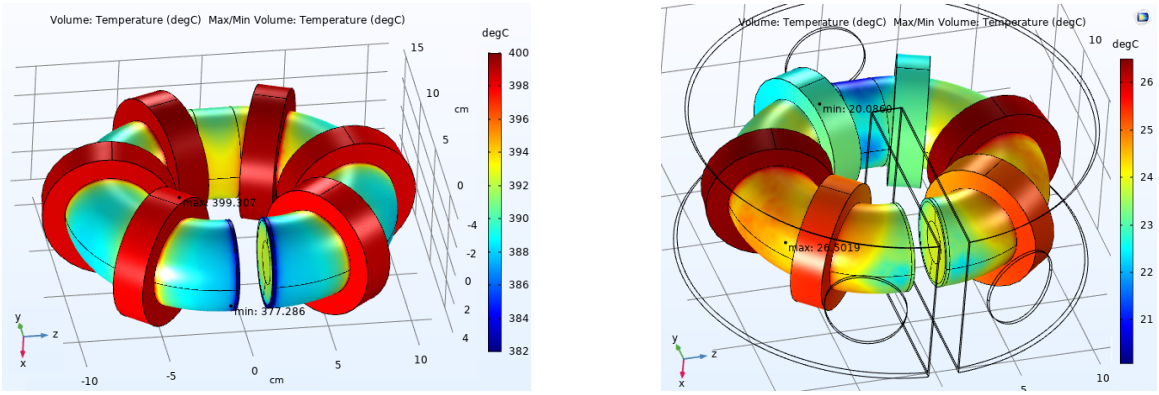

(a) (b)

FIG. 9. Volumetric temperature plot of the fillings core magnet system (with customized poles). Equilibrium temperature **(a)** without cooling and **(b)** with cooling. In **(b)**, note the casing around the magnet system, where the air flow entry (a fan in the back) and exits (two grilles near the gap) can be seen.

VIII. MAGNET ASSEMBLY AND EXPERIMENTAL RESULTS

After establishing the most suitable magnet configurations for the intended objectives, and analysing their characteristics, the two magnet systems were assembled.

A. Fillings Core Magnet

The prototype of this magnet system is composed of three distinct components: the coils, the ferromagnetic core made of iron fillings and the plastic casing where the fillings are placed. Each coil is comprised of 146 turns of copper wire with 1.28 mm diameter (see Fig. 10 **(a)**). The casing was created using a 3D printer, and was made of 2 mm thick plastic (PLA) filament. In order to allow for the insertion of the iron fillings, the casing was printed in halves. A locking mechanism was added to its interior to help connect the two halves, and keep the casing from opening. As for the iron fillings, they were outsourced in a metal factory. Inside the casing, they had to be compacted as much as possible to minimize the presence of air between particles (see Fig. 10 **(b)**). In fact, ideally, the iron fillings should act as a solid iron core, since this would maximize the relative permeability of the core, and therefore, for a given current, the intensity of the field in the gap.

After assembling the magnet system, and performing all the necessary electrical connections (particularly, connecting the coils to the power source), it was possible to start executing experimental tests. Before anything else, it was necessary to ensure that a magnetic field of 0.21 T was achievable in the middle of the gap, since failure to do so would immediately tell us that this solution was not viable. Using a Hall sensor, field measurements were then performed in the gap, which revealed that the field intensity was nowhere close to the expected value, being about 100 times lower than 0.21 T. The poor results obtained were explained by the lack of compactness of the iron fillings in the core. In fact, the core weight was only, approximately, 1.30 kg, while the weight of a perfectly compact core should be 6.20 kg. This meant that a significant amount of air was "stuck" inside the casing, which drastically reduced the relative permeability of the iron core, and therefore the intensity of the field in the gap.

(a) (b)

FIG. 10. Detail of **(a)** one of the assembled coils and **(b)** the iron fillings compacted inside half of the core.

As there was no realistic way of being able to further compact the fillings inside the casing since we were already at the limit of our technical capacities, the solution of developing a magnet system using an iron fillings core was promptly disregarded.

B. Laminated Core Magnet

To create the prototype of the laminated core magnet system only two components are required: the coils (similar to the ones used for the fillings core magnet) and the thin iron plates (sheets), known as laminations. The laminated core (see Fig. 11 **(a)**) was outsourced to a metal

factory, and was composed of 0.5 mm thick iron sheets.

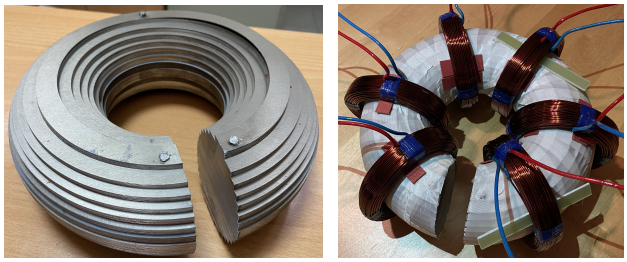

(a) (b)

FIG. 11. **(a)** Laminated core. **(b)** Assembled magnet system.

Due to some unforeseen delays in the manufacture and assembly of the laminated magnet system, it was not yet possible to perform all the desired experimental tests. The only test done so far was a measurement of the induced field in the middle of the gap as a function of the current applied to the coils, whose results are presented in Fig. 12.

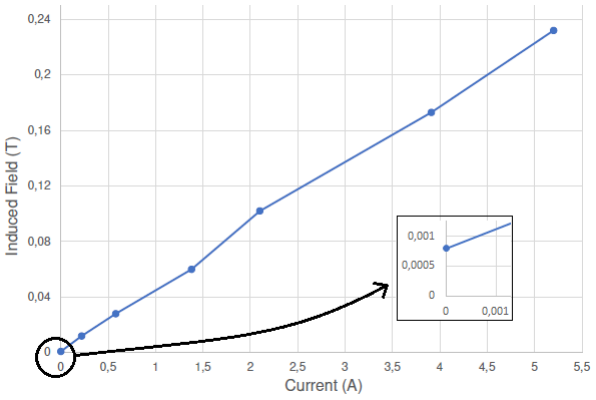

FIG. 12. Evolution of the induced field in the middle of the gap as a function of the current applied to the coils. Note the existence of a small residual field.

These preliminary results agree well with the expected. Because of this, and since this is an approach successfully employed in the past, we are confident that as we continue testing this magnet the results will be satisfactory, which will allow us to conclude that this is a viable solution.

IX. CONCLUDING REMARKS

An innovative FFC NMR magnet system was successfully designed with the purpose of enhancing the relaxometer's usability, by increasing its portability capacities. Two solutions in terms of the magnet's core composition were tested and fully characterized in terms of their field homogeneity, fringing effect and heating/cooling effects.

It was possible to disregard the approach of using iron fillings to form the magnet's core since, from a technical standpoint, it was not feasible to develop this magnet with the desired characteristics.

As for the approach of using a laminated core, due to some unforeseen delays out of our control, it was not yet possible to fully test the laminated core magnet. Nonetheless, preliminary test results seem to agree with expectation. More tests will be performed in the near future, which will include the measurement of coils characteristics such as their resistance and inductance, the calculation of the fringing effect, and particularly a 3D mapping of the induced field in the gap to confirm if the simulated field homogeneity is realistic.

Relatively to other FFC magnets, the main advantages of the designed magnet are: the reduced volume (and weight); the high homogeneity of the induced field in the gap region; the low power demands; and the ability to have complete freedom of rotation in all three axes. All these advantages contribute heavily to the increase of the relaxometer's portability capacities and, if proven experimentally, will allow to develop the first portable FFC relaxometer, thus proving a new concept in FFC NMR relaxometry.

[1] M. H. Levitt, *Spin dynamics: basics of nuclear magnetic resonance* (John Wiley & Sons, 2013).

[2] F. Fujara, D. Kruk, A. F. Privalov, *Progress in nuclear magnetic resonance spectroscopy* **82**, 39 (2014).

[3] D. M. Sousa, G. D. Marques, J. M. Cascais, P. J. Sebastiao, *Solid State Nuclear Magnetic Resonance* **38**, 36 (2010).

[4] W. Veeman, *Geoderma* **80**, 225 (1997).

[5] R. Kimmich, E. Anoardo, *Progress in Nuclear Magnetic Resonance Spectroscopy* **44**, 257 (2004).

[6] A. Abragam, *The Principles of Nuclear Magnetism* (Oxford university press, 1961).

[7] P. J. Hore, *Nuclear Magnetic Resonance* (Oxford University Press, USA, 2015).

[8] T. C. Farrar, E. D. Becker, *Pulse and Fourier transform NMR: Introduction to Theory and Method* (Elsevier, 2012).

[9] F. Bloch, *Physical review* **70**, 460 (1946).

[10] Relaxation (NMR), `https://en.wikipedia.org/wiki/Relaxation_(NMR)`. Accessed: 29-04-2020.

[11] F. Noack, *Progress in nuclear magnetic resonance Spectroscopy* **18**, 171 (1986).

[12] E. Anoardo, G. Galli, G. Ferrante, *Applied Magnetic Resonance* **20**, 365 (2001).

[13] R. Kimmich, *NMR: Tomography, Diffusometry, Relaxometry* (Springer Science & Business Media, 2012).

[14] A. Roque, Espectrometro de rmn de ccr com utilizao de supercondutores no magneto, Ph.D. thesis, IST (2014).

[15] P. Videira, Fast-field cycling nuclear magnetic resonance relaxometer's magnet with optimized homogeneity and reduced volume (2017).